AIMS Mathematics, 8(8): 19097–19120.
DOI: 10.3934/math.2023975
Received: 16 January 2023
Revised: 24 May 2023
Accepted: 25 May 2023
Published: 07 June 2023

http://www.aimspress.com/journal/Math

Research article

Short-memory discrete fractional difference equation wind turbine model and its inferential control of a chaotic permanent magnet synchronous transformer in time-scale analysis

Abdulaziz Khalid Alsharidi[1], Saima Rashid[2,*] and S. K. Elagan[3,4]

[1] Department of Mathematics and Statistics, College of Science, King Faisal University, Al-Hasa 31982, Saudi Arabia

[2] Department of Mathematics, Government College University, Faisalabad 38000, Pakistan

[3] Department of Mathematics and Statistics, College of Science, Taif University, P.O. Box 11099, Taif 21944, Saudi Arabia

[4] Department of Mathematics and Computer Sciences, Faculty of Science Menoufia University, Shebin Elkom, Egypt

* **Correspondence:** Email: saimarashid@gcuf.edu.pk.

Abstract: The aerodynamics analysis has grown in relevance for wind energy projects; this mechanism is focused on elucidating aerodynamic characteristics to maximize accuracy and practicability via the modelling of chaos in a wind turbine system's permanent magnet synchronous generator using short-memory methodologies. Fractional derivatives have memory impacts and are widely used in numerous practical contexts. Even so, they also require a significant amount of storage capacity and have inefficient operations. We suggested a novel approach to investigating the fractional-order operator's Lyapunov candidate that would do away with the challenging task of determining the indication of the Lyapunov first derivative. Next, a short-memory fractional modelling strategy is presented, followed by short-memory fractional derivatives. Meanwhile, we demonstrate the dynamics of chaotic systems using the Lyapunov function. Predictor-corrector methods are used to provide analytical results. It is suggested to use system dynamics to reduce chaotic behaviour and stabilize operation; the benefit of such a framework is that it can only be used for one state of the hybrid power system. The key variables and characteristics, i.e., the modulation index, pitch angle, drag coefficients, power coefficient, air density, rotor angular speed and short-memory fractional differential equations are also evaluated via numerical simulations to enhance signal strength.

Keywords: permanent magnet synchronous generator; chaotic system; Lyapunov function; equilibrium points; short-memory; time-scale analysis

Mathematics Subject Classification: 46S40, 47H10, 54H25

1. Introduction

In recent years, the amount of turbine-sourced electricity produced has risen dramatically to safeguard the planet from the effects of anthropogenic emissions and fossil fuel use [1]. The potential energy of the airflow is converted by the wind farm into mechanical energy, which is later transformed into electric power. Part of the offshore airflow is captured by the control surfaces and transferred to the connector, which is then be rectified to the jet stream turbine's motor. The electro-mechanical system then receives the mechanical energy and transforms it into electricity that is generated [2].

There are numerous power station components including some coupled inductors [3], an electrically excited synchronous transformer [4] and a permanent magnet synchronous generator (PMSG) [5]. Due to the PMSG's numerous benefits, including its moderate value of production, top bandwidth, sturdiness, ease of fabrication, fast response, operation at maximum power point, and high power density, it is an attractive implementation transformer for use in conjunction with a power system, and it is well-known in the market as one of the most encouraging wind configurations.

The PMSG is a classic dynamic, nonlinear, interacting framework and even if the input propeller, including an impact field, is successfully completed, its effectiveness is acutely vulnerable to boot-up perturbations, surface roughness and specification variability. According to several explorations, the PMSG exhibits chaotic behaviour whenever the active disturbance rejection control strategy is proposed. The implementation of a predictive control strategy is being examined with a one-point controller of PMSG, and this control technique that employs genetic algorithms to determine the most effective parameter values of the wind turbine results in energy generation maximisation [6]. Due to all of these elements, it is stressful to manage the PMSG in order to achieve flawless monitoring progress characteristics in practical applications. In the area of adaptive dynamics of the power source, the marginalisation and regulation of upheaval in a PMSG have drawn a lot of interest. For the downregulation and management of chaos in a PMSG, different switching techniques have been constructed to date [7].

Fractional-order (FO) calculus is a significant area of mathematics that was developed nearly simultaneously with classical integer-order calculus. L'Hospital and Leibnitz corresponded about the significance of the derivative of order 0.5 in 1695. Due to the ambiguity surrounding the strong relevance of FO derivatives and its applications, FO calculus has been constructed for three decades primarily as pure mathematics [8, 9]. Interestingly, the memory and/or nonlocality of the framework can fluctuate with time, space, or additional factors, according to the research [10]. The memory and hereditary characteristics associated with numerous tangible processes and events can be described using the variable-order (VO) fractional operators and their non-stationary power-law kernel. As a result, VO fractional calculus emerged as an intriguing option for establishing a viable mathematical scheme for perfectly identifying multifaceted physical structures and procedures [11]. Following that, VO-fractional differential equations (FDEs) gained growing interest, owing to their appropriateness for modelling a wide range of phenomena, including those related to anomalous diffusion, viscoelastic mechanics, control systems, petroleum engineering and numerous additional areas of

science and technology. In 1993, Samko and Ross [12] put forward the notion of VO integrals and differentials, in addition to some basic features. Lorenzo and Hartley [13] summarized the VO fractional operator study findings and then examined the terminology of VO fractional operators in different contexts. Following that, certain novel variations and important implementation potentials of the VO-FDE models were additionally investigated [14]. In the past decade, VO-FDE has emerged as an epicentre for research and has sparked broad concern. VO-FDEs have rapidly advanced over the last few centuries in terms both the mathematical approach and practical implementation [15, 16]. In this investigation, we use Caputo FO and VO calculus because it provides a significant advantage in terms of removing the restrictions on the primitive function [8, 9, 14]. An essential component to characterize the size of the memory is the FO feature. The currently used "derivative" ${}_{\xi_0}^{c}\mathbb{D}_{\xi}^{\varphi}$ is the continuous concentration of the classical derivative $\phi'(\xi)$ from the starting point of ξ_0 to ξ.

Fractional difference equations are effective models for discrete processes with memory effects. Several specific advancements, such as the Riemann and Caputo fractional differences, the fundamentals of discrete fractional calculus, numerical simulations, initial value problems, etc., demonstrate this viewpoint [17]. Implementations of discrete fractional calculus, such as those involving fractional chaotic maps, image encryption, tumour growth and shock frequency, among others, further demonstrate its effectiveness and simplicity [18, 19].

In the real sense, Miller and Ross [8] classified a fractional sum by expanding linear difference equations in 1981 as follows:

$$\Delta^{-\varphi}\mathbf{g}(\xi) = \frac{1}{\Gamma(\varphi)}\sum_{\mathbf{s}=\mathbf{a}+\varphi}^{\xi}\frac{\Gamma(\xi-\mathbf{s}+\varphi)}{\Gamma(\xi-\mathbf{s}+1)}\mathbf{g}(\mathbf{s}-\varphi), \quad \xi \in \mathbb{N}_{\mathbf{a}+\varphi}. \tag{1.1}$$

Therefore, (1.1) can be assumed to be the discrete form of the Riemann-Liouville fractional integral. The semi-group property of the fractional sum, for instance, is an underlying scientific theory that is challenging to introduce within the context of classical discrete calculus. Perhaps because of this, fractional difference equations have received too little consideration.

Another approach to determining the fractional sum is on the basis of time scale [20]. Both the continuous and discrete-time incidences were generalized. In addition to the Δ-integral on time scales, better characterizations for the mathematical framework were provided [21]. Guo et al. [22] contemplated the three-dimensional fractional total variation regularized tensor optimized model for image deblurring. The FO φ better describes the transitional state between interfacial tension and pliability. A methodology based on FDEs is presented in [18], showing that sodium chloride exhibits long-term memory behaviour. In addition, there are a few other fascinating fields where fractional derivatives are used, including finance, biology and string theory. Several other fractional formulae have been suggested, including fractional delay differential equations, fractional impulsive differential equations, fractional interval-valued differential equations and fractional difference equations (see [19, 23–25] and the references cited therein). Fractional calculus has grown in popularity as a modelling technique.

As a result, fractional operators have a significant impact on scientific methods for processes and systems such as the memristor [26], electroosmotic slip flow of Oldroyd-B fluid [27] and (PMSM) models [4].

However, PMSM's effectiveness is impacted by plant-wide exterior capacity disturbances and model parameters. Several studies, like those by Li et al. [28] and Jing et al. [29], demonstrate that the

PMSM exhibits chaotic behaviour when specific input parameters are used. It has been discovered that several processes in multiple disciplines can be eloquently explained with the aid of fractional derivatives [12, 13]. Integer-order (classical) DEs are merely a special case of FDEs, which are used to describe all observed processes in existence [30]. FO and VO frameworks are significant because they can produce a more appropriate version and provide a profound understanding of the physical mechanisms underpinning long-term memory behaviour. Numerous fields of scientific research and construction have used chaos simulation [31].

The article is organized as follows, in Section 2, we first deduce the integer-order dimensionless framework of the PMSG wind turbine structure. Utilising a discrete Caputo fractional derivative, the PMSG system's FO concept is created in Section 3. In Section 4, a design procedure for the FO-PMSG scheme is developed to demonstrate its chaotic behaviour. Furthermore, a FO responsive control scheme is created to reduce the variability of the FO-PMSG mechanism. Section 4 also deduces the consistency of the device. The generated device's ability to restrict chaotic oscillations is demonstrated through simulation studies.

2. Mathematical modelling of the wind turbine

Because wind is an infinitely sustainable option, harnessing its kinetic energy has no influence on the intrinsic processes that cause turbines to turn. Because of this, using renewable energy is significantly more ecologically friendly than power generation by the combustion of fossil fuels, and wind generators create power without harming the environment as the wind passes. In this context, an induction motor with synchronous machines and turbines is a highly complex electric power-generating system that includes metal equipment, a differential velocity generator and a simple end-up driving of the transformer. This intricate electric power-generating structure is shown in [4].

In order to satisfy the conditions of the specialised formulae required for the system shown in Figure 1, we will describe the following: $\wp_{1\mathbf{abc}}$, which stands for capacity resistance, $\wp_{\mathbf{sabc}}$, which denotes the generator's three-phase circuit, $\mathbf{v_{dc}}$, which denotes the voltage level, $\mathbf{v_{sabc}}$, which denotes the rotor circuit three-phase battery, $\mathcal{Q}_\varepsilon$ and $\mathcal{P}_\varepsilon$, which denotes the proactive and reactive power density, respectively, $\mathbf{v}$, which stands for airflow, β, which is the infield viewpoint, and $\mathcal{P}_\mathbf{w}$, which stands for the power consumed by the airflow. The basic mathematical formulation for wind power can be converted into mechanical power. described in the following way:

$$\mathcal{P}_\mathbf{w} = \frac{\pi}{2}\rho C_\mathcal{P} \mathbf{v}_\mathbf{w}^3 \mathcal{R}^2. \tag{2.1}$$

The formula for the modulation index that represents aerodynamic effectiveness is

$$C_\mathcal{P}(\varsigma, \beta) = (\Lambda\zeta_1\zeta_2 - \beta\zeta_1\zeta_3 - \zeta_1\zeta_4)\exp(-\Lambda) + \varsigma\zeta_6, \tag{2.2}$$

where $\Lambda = \left(\frac{1}{\varsigma+0.05\beta} - \frac{0.035}{\beta^3+1}\right)$. Table 1 lists the operational specifications for (2.1) and (2.2).

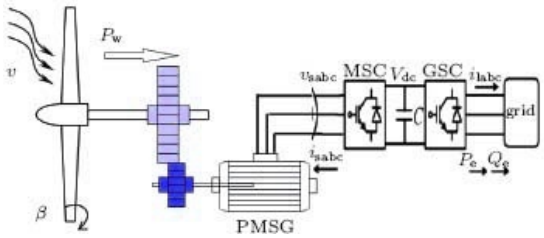

(a)

Figure 1. Wind turbine with a PMSG [4].

Table 1. List of parameters.

Symbols	Explanation
ρ	Air density
$C_{\mathcal{P}}$	Power coefficient
$\ell_{\mathbf{w}}$	Wind speed
$\mathcal{R}$	Turbine
ς	Tip speed ratio
β	Pitch angle
Λ	Assumed variable
$\zeta_1 - \zeta_6$	Drag coefficients
ω	Rotor angular velocity

Drag coefficients $\zeta_1 = 0.5109, \zeta_2 = 116, \zeta_3 = 0.4, \zeta_4 = 5, \zeta_5 = 21$, and $\zeta_6 = 0.068$ are also shown. The following formulas are used to describe the rotor's angular velocity:

$$\varsigma = (\mathbf{v_w})^{-1}\mathcal{R}\omega. \tag{2.3}$$

Furthermore, (2.1) is used to solve (2.2) and (2.3), and the result is

$$\mathcal{P}_{opt} = \frac{\pi}{2}\rho C_{\mathcal{P}}\mathbf{v}_{\mathbf{w}}^3\mathcal{R}^2 C_{\mathcal{P}} \max\Big(\frac{\mathcal{R}^3\omega^3}{\varsigma_{opt}^3}\Big). \tag{2.4}$$

We now deduce the fundamental interacting voltage formulae using the 3ϕ and 2ϕ stationarity of the variables with respect to two components, i.e., a static structure ψ, three-phase abc stationary to two-phase **a** and a ψ stationary reference frame as follows:

$$\mathbf{v}_\chi = \mathbf{v_a} - \frac{1}{2}(\mathbf{v_b} + \mathbf{v_c}), \quad \mathbf{v}_\psi = \frac{\sqrt{3}}{2}(\mathbf{v_b} - \mathbf{v_c}) \tag{2.5}$$

and

$$\mathbf{v_d} = \mathbf{v}_\psi \sin\vartheta + \mathbf{v}_\chi \cos\vartheta, \quad \mathbf{v_r} = \mathbf{v}_\psi \cos\vartheta - \mathbf{v}_\chi \sin\vartheta. \tag{2.6}$$

Now, we investigate the PMSG wind turbine's final efficiency and prevailing interactions by attempting to solve (2.5) and (2.6) as

$$\begin{cases} \dot{\omega} = \frac{\mathbf{p}}{J}[\iota_{\mathbf{r}}\phi_{\mathbf{g}} + \iota_d i_{\mathbf{r}}(\bar{L}_{\mathbf{d}} - \bar{L}_{\mathbf{r}})] - \frac{\bar{T}_{\bar{L}}}{J} - \omega\frac{\bar{F}}{J}, \\ \hat{\iota}_{\mathbf{r}} = \frac{\mathbf{v}_{\mathbf{r}}}{\bar{L}_{\mathbf{d}}} - \frac{\mathcal{R}_{\mathbf{s}}}{\bar{L}_{\mathbf{r}}}\iota_{\mathbf{r}} - \frac{\rho\phi_{\mathbf{g}}}{\bar{L}_{\mathbf{r}}}\omega + \omega\rho\iota_{\mathbf{d}}\frac{\bar{L}_{\mathbf{d}}}{\bar{L}_{\mathbf{r}}}, \\ \hat{\iota}_{\mathbf{d}} = \frac{\mathbf{v}_{\mathbf{r}}}{\bar{L}_{\mathbf{d}}} - \frac{\mathcal{R}_{\mathbf{s}}}{\bar{L}_{\mathbf{r}}}\iota_{\mathbf{r}} + \omega\rho\iota_{\mathbf{d}}\frac{\bar{L}_{\mathbf{d}}}{\bar{L}_{\mathbf{r}}}. \end{cases} \tag{2.7}$$

Here, $\mathcal{P}$ represents the quantity of pole sets, $\mathbf{g}$ is the tension factor, J is the inertial moment of the turbine, $\bar{T}_{\bar{L}}$ stands for the load rotational speed, $\phi_{\mathbf{g}}$ denotes the rotor speed latching mechanism with the transformer, $\mathcal{R}_{\mathbf{s}}$ is the stator resistance, $\bar{L}_{\mathbf{r}}$ denotes the phase difference, $\iota_{\mathbf{r}}$ and $\iota_{\mathbf{d}}$ are the quadrature and direct axis stator currents, $\mathbf{v}_{\mathbf{r}}$ indicates the phase shift and $\mathbf{L}_{\mathbf{d}}$ is the viscous friction coefficient. Now, using (2.7), which describes the aerodynamic framework of a wind generator manufactured by the authors of [4], compute the following non-dimensional quantities:

$$\begin{cases} \dot{\mathbf{x}} = \delta_1(\mathbf{y} - \mathbf{x}) + \delta_2\mathbf{yz}, \\ \dot{\mathbf{y}} = \delta_3\mathbf{x} - \mathbf{xz} - \mathbf{y}, \\ \dot{\mathbf{z}} = \mathbf{xy} - \mathbf{z}. \end{cases} \tag{2.8}$$

We specify the presented interpretations of the short-memory fractional differential/integral formulations in [32] in order to formulate the mathematical aerodynamic framework of a wind generator using these interpretations.

In this article, we just take into account the fractional derivatives of the Caputo type. Following that, we describe short-term memory fractional derivatives and explain their purpose.

Definition 2.1. ([33, 34]) For $\varphi > 0$, suppose that there is a mapping $\phi \in \mathcal{L}^1([\xi_0, \mathbb{T}]; [R])$. Then the Riemann-Liouville integral operator is stated as

$${}_{\xi_0}\mathbb{I}^{\varphi}_{\xi}\phi(\xi) = \frac{1}{\Gamma(\varphi)}\int_{\xi 0}^{\xi}(\xi - \mathbf{s})^{\varphi-1}\phi(\mathbf{s})d\mathbf{s},\ \xi \in [\xi_0, \mathbb{T}], \tag{2.9}$$

where $\Gamma(,)$ denotes the Euler-gamma function.

Definition 2.2. ([33, 34]) For $\varphi \in (0, 1]$, suppose that there is a mapping $\phi \in \mathcal{L}^1([\xi_0, \mathbb{T}]; [R])$. Then the Riemann-Liouville derivative operator for ϕ is stated as

$${}_{\xi_0}\mathbb{D}^{\varphi}_{\xi}\phi(\xi) = \frac{d}{d\xi}\mathbb{I}^{1-\varphi}_{\xi}\phi(\xi),\ \textit{almost everywhere}\ \xi \in [\xi_0, \mathbb{T}]. \tag{2.10}$$

Definition 2.3. ([33, 34]) For $\varphi \in (0, 1]$, suppose that there is a mapping $\phi \in \mathcal{L}^1([\xi_0, \mathbb{T}]; [R])$ such that ${}_{\xi_0}\mathbb{D}^{\varphi}_{\xi}\phi(\xi)$ holds for almost everywhere $\xi \in [\xi_0, \mathbb{T}]$. The Caputo derivative operator for ϕ is stated as

$${}^{c}_{\xi_0}\mathbb{D}^{\varphi}_{\xi}\phi(\xi) = {}_{\xi_0}\mathbb{D}^{\varphi}_{\xi}[\phi(\xi) - \phi(\xi_0)],\ \textit{almost everywhere}\ \xi \in [\xi_0, \mathbb{T}]. \tag{2.11}$$

Remark 2.1. If $\phi(\xi)$ is differentiable, then

$${}^{c}_{\xi_0}\mathbb{D}^{\varphi}_{\xi}\phi(\xi) == \frac{1}{\Gamma(1-\varphi)}\int_{\xi_0}^{\xi}(\xi - \mathbf{s})^{-\varphi}\phi'(\mathbf{s})d\mathbf{s},\ \varphi \in (0, 1) \tag{2.12}$$

and ${}^{c}_{\xi_0}\mathbb{D}^{\varphi}_{\xi}\phi(\xi) = \frac{d\phi}{d\xi}$ for $\varphi = 1$.

What follows are certain additional fractional derivatives that resemble Caputo.

Definition 2.4. ([35]) For $\ell > 0$ and $\mathbf{a} \in \mathbb{R}$, suppose that $\mathbf{g} : \mathbb{N}_{\mathbf{a}} \mapsto \mathbb{R}$. Then the ℓth-order fractional sum is presented as

$$\nabla_{\mathbf{a},\hbar}^{-\ell}\mathbf{g}(\xi) := \frac{\hbar}{\Gamma(\ell)} \sum_{\mathbf{s}=\mathbf{a}/\hbar}^{\frac{\xi}{\hbar}-\ell} (\xi - \sigma(\mathbf{s}\hbar))^{(\ell-1)}\mathbf{g}(\mathbf{s}\hbar), \;\; \sigma(\mathbf{s}) = \mathbf{s} + \hbar, \; \xi \in (\hbar\mathbb{N})_{\mathbf{a}+\ell\hbar}, \tag{2.13}$$

where $\xi_{\hbar}^{(\ell)} = \hbar^{\ell}\frac{\Gamma(\frac{\xi}{\hbar}+1)}{\Gamma(\frac{\xi}{\hbar}+1-\ell)}$ denotes the discrete factorial function.

Definition 2.5. ([36]) For $\ell \in (0, 1]$ and $\mathbf{a} \in \mathbb{R}$, suppose that $\mathbf{g} : \mathbb{N}_{\mathbf{a}} \mapsto \mathbb{R}$. Then the ℓth-order Caputo fractional difference is presented as

$${}^{c}\nabla_{\mathbf{a},\hbar}^{\ell}\mathbf{g}(\xi) := \frac{\hbar}{\Gamma(1-\ell)} \sum_{\mathbf{s}=\mathbf{a}/\hbar}^{\frac{\xi}{\hbar}+\ell-1} (\xi - \sigma(\mathbf{s}\hbar))^{(-\ell)}\nabla_{\hbar}\mathbf{g}(\mathbf{s}\hbar), \quad \mathbf{a} \in \mathbb{R}, \; \xi \in \mathbb{N}_{\mathbf{a}+(1-\ell)\hbar}, \tag{2.14}$$

and ${}^{c}\nabla_{\mathbf{a},\hbar}^{\ell}\mathbf{g}(\xi) = \nabla_{\hbar}\mathbf{g}(\xi)$ for $\ell = 1$.

The interpretations mentioned above are classical fractional derivatives and differences involving long-memory impacts beginning at time ξ_0 or $\mathbf{a}$.

Definition 2.6. ([37]) For $\ell(\xi) \in (0, 1]$, $\mathbf{t} \in \mathbb{N}_{\mathbf{a}}$ and suppose that $\mathbf{g} : \mathbb{N}_{\mathbf{a}} \mapsto \mathbb{R}$. Then the ℓth-VO Caputo fractional difference is presented as

$${}^{c}\nabla_{\mathbf{a},\hbar}^{\ell(\xi)}\mathbf{g}(\xi) := \frac{\hbar}{\Gamma(1-\ell(\xi))} \sum_{\mathbf{s}=\mathbf{a}/\hbar}^{\frac{\xi}{\hbar}+\ell-1} (\xi - \sigma(\mathbf{s}\hbar))^{(-\ell(\xi))}\nabla_{\hbar}\mathbf{g}(\mathbf{s}\hbar), \quad \mathbf{a} \in \mathbb{R}, \; \xi \in \mathbb{N}_{\mathbf{a}+(1-\ell(\xi))\hbar}. \tag{2.15}$$

3. Short-memory principle

The short-memory principle (also known as the fixed memory principle or the logarithmic memory principle) is approached from a new perspective, and as a result, its efficiency is increased from $\varphi \in (0, 1)$ to $\varphi \in (0, 2)$, which is also related to the observation that case $\varphi \geq 2$ does not appear to be particularly pragmatic. When $\varphi \in (0, 1)$, the kernel decays much more quickly and exhibits Podlubny's fixed memory principle. For the application of the fixed memory principle and its useful applications, (see [33, 38]).

$${}_{\xi_0}^{C}\mathbb{D}_{\xi}^{\varphi}\mathbf{x}(\xi) = \mathbf{g}(\mathbf{x}, \xi), \tag{3.1}$$

where ${}_{\xi_0}^{C}\mathbb{D}_{\xi}^{\varphi}\mathbf{x}(\xi) \approx {}_{\xi-\bar{L}}^{C}\mathbb{D}_{\xi}^{\varphi}\mathbf{x}(\xi)$. Numerical methodologies use only data from $\mathbf{x}(\xi - \bar{L})$ to $\mathbf{x}(\xi)$, resulting in less data to store and a significant reduction in supercomputing costs. In actuality, we might run into the following challenges when using fractional calculus in practical situations:
(a) Remember that the framework of the medium and its components may vary or be significantly altered [39]. The modelling process does not require any historical data. After that, memory only begins at the innovative phase.

(b) By using simulation tools for fractional chaotic processes, chaotic series development raises simulation complexity [40, 41]. As a result, creating accelerated encrypted communication algorithms and protecting large amounts of personal content are difficult.
(c) Effectiveness and algorithmic efficiency should be balanced in other fractional modelling implementations.

Here, we have the accompanying main memory FDEs to tackle these issues and are incentivized by the well-known fixed memory principle [33, 38] as follows:

$$\begin{cases} {}^{c}_{\xi-\bar{L}}\mathbb{D}^{\varphi}_{\xi}\mathbf{x}(\xi) = \mathbf{g}(\mathbf{x},\xi), \;\; \bar{L} > 0, \\ \mathbf{x}(\xi) = \psi(\xi), \;\; \xi \in [\xi_0 - \bar{L}, \xi_0], \; \varphi \in (0,1] \end{cases} \tag{3.2}$$

and

$$\begin{cases} {}^{c}_{\xi^*}\mathbb{D}^{\varphi}_{\xi}\mathbf{x}(\xi) = \mathbf{g}(\mathbf{x},\xi), \;\; \bar{L} > 0, \\ \mathbf{x}(\xi_0) = \mathbf{x}_0, \;\; \xi^* = \xi_\kappa, \xi^*, \xi \in [\xi_0 \mathbb{T}], \;\; \kappa = 0, ..., \mathfrak{m}. \end{cases} \tag{3.3}$$

Regarding the initial setting ξ^* in the fractional derivative, we will now have different occurrences:
Case I: When $\xi^* \mapsto \xi_0$, then (3.3) is transformed into the classical FDEs containing long memory.
Case II: In (3.3), when $\bar{L} \mapsto 0$ *or* $\xi^* \mapsto \xi$ in (3.2), produces

$$\mathbb{D}^{\varphi}_{\xi}\phi(\xi) = \lim_{\bar{L}\mapsto 0} {}^{c}_{\xi-\bar{L}}\mathbb{D}^{\varphi}_{\xi}\phi(\xi) \tag{3.4}$$

and

$$\mathbb{D}^{\varphi}_{\xi}\phi(\xi)\Big|_{\xi=\xi^*} = \lim_{\xi\mapsto\xi^*} {}^{c}_{\xi^*}\mathbb{D}^{\varphi}_{\xi}\phi(\xi), \tag{3.5}$$

respectively. They are members of the class of local fractional derivatives [42], rendering the framework local and memoryless.
Case III: The relationship between locality and long memory for time $\xi^* \in (\xi_0, \xi)$ is a feature of the scheme (3.3). Here, we consider it to have a fixed memory.

There are two major differences between the fixed memory FDEs: unlike (3.2), which has a fixed constant length of $\bar{L}$, (3.3) has variable memory.

A further advancement is VO FC. This concept was used by Sun et al. [43] in their fractional modelling of propagation through complicated media. For instance, the VO fractional derivative is identified by

$${}^{c}_{\xi_0}\mathbb{D}^{\varphi(\xi)}_{\xi}\phi(\xi) = \frac{1}{\Gamma(1-\varphi(\xi))}\int_{\xi_0}^{\xi}(\xi-\mathbf{s})^{-\varphi(\mathbf{s})}\phi'(\mathbf{s})d\mathbf{s}, \;\; \xi_0 < \xi, \; \varphi(\xi) \in (0,1], \tag{3.6}$$

where $\varphi(\xi)$ is a function whose value depends on ξ. It can be viewed as being a more prevalent instance of (2.10). Numerous different fractional VO methodologies have been introduced, and it is advantageous to acquire the analytical results by using predictor-corrector techniques [44]. For instance, the VO fractional integral is identified by

$${}_{\xi_0}\mathbb{I}^{\varphi(\xi)}_{\xi}\phi(\xi) = \frac{1}{\Gamma(\varphi(\xi))}\int_{\xi_0}^{\xi}(\xi-\mathbf{s})^{\varphi(\mathbf{s})-1}\phi'(\mathbf{s})d\mathbf{s}, \;\; \xi_0 < \xi, \; \varphi(\xi) \in (0,1]. \tag{3.7}$$

Moreover, the Leibniz rule and semi-group characterization do not satisfy certain well-noted formulae in the FC:

$$\begin{aligned} &{}_{\xi_0}\mathbb{I}_{\xi}^{\varphi(\xi)}\,{}_{\xi_0}^{c}\mathbb{D}_{\xi}^{\varphi(\xi)}\phi(\xi) = \phi(\xi) - \phi(0), \;\; \xi > \xi_0, \; \varphi(\xi) \in (0,1], \\ &{}_{\xi_0}^{c}\mathbb{D}_{\xi}^{\varphi(\xi)}\,{}_{\xi_0}\mathbb{I}_{\xi}^{\varphi(\xi)}\phi(\xi) = \phi(\xi), \;\; \xi > \xi_0, \; \varphi(\xi) \in (0,1] \end{aligned} \tag{3.8}$$

and

$${}_{\xi_0}\mathbb{I}_{\xi}^{\varphi(\xi)}\,{}_{\xi_0}\mathbb{I}_{\xi}^{\beta(\xi)} = {}_{\xi_0}\mathbb{I}_{\xi}^{\varphi(\xi)+\beta(\xi)}\phi(\xi), \; \xi > \xi_0, \;\; \varphi(\xi), \beta(\xi) > 0. \tag{3.9}$$

As a result, the emergence consequences and certain other conceptual components that use the corresponding integral equations to specify fixed-point formulations cannot be considered. Having a VO strategy that is practical and feasible for both qualitative and numerical modelling is becoming a difficult task. An FDE containing a VO can be defined for the fixed memory scenario. With respect to ξ, the FO mapping can be thought of as a piecewise constant mapping. We only take into account the fixed memory FDE from the aforementioned evaluation of the fixed memory and VO technique (3.3). We exclusively employ the Caputo-type derivative or difference scheme in this investigation because the Riemann-Liouville derivative necessitates integral initial conditions (ICs).

3.1. Short-memory and fractional VO technique for modelling

Initially, we introduce the spatial solution for (3.3). At ξ_κ, if $\mathbf{x}(\xi_\kappa^-) = \mathbf{x}(\xi_\kappa^+)$, then the continuous findings can be illustrated, whereas $\mathbf{x}(\xi_\kappa^-) \neq \mathbf{x}(\xi_\kappa^+)$ yields a fractional impulsive DEs. We use impulsive FDE representations [45]. Suppose there is a Banach space $\mathbb{C}(\mathcal{J}, \mathbb{R})$ of all continuous functions having the norm $\|\mathbf{u}\|_c := \sup\{\|\mathbf{u}\| : \xi \in \mathcal{J} = [\xi_0, \mathbb{T}]\}$. For $0 = \xi_0 < \xi_1 < ... < \xi_{\mathfrak{m}} < \xi_{\mathfrak{m}+1} = \mathbb{T}$, the set $\mathbb{C}(\mathcal{J}, \mathbb{R}) = \{\mathbf{u} : \mathcal{J} \mapsto \mathbb{R} : \mathbf{u} \in \mathbb{C}(\xi_\kappa, \xi_{\kappa+1}], \mathbb{R}), \kappa = 0, ..., \mathfrak{m}\}$ is also a Banach space with $\mathbf{u}(\xi_\kappa^+) = \lim_{\epsilon \mapsto 0^+} \mathbf{u}(\xi_\kappa + \epsilon)$ and $\mathbf{u}(\xi_\kappa^-) = \lim_{\epsilon \mapsto 0^-} \mathbf{u}(\xi_\kappa + \epsilon)$.

Wu et al. [32] demonstrated the idea of fixed-memory FDEs. For $\xi \in [\xi_0, \xi_1]$, we have the FDE ${}_{\xi_0}^{c}\mathbb{D}_{\xi}^{\varphi_0}\mathbf{x} = \mathbf{g}(\mathbf{x}, \xi)$. At time ξ_1, for $\xi \in (\xi_1, \xi_2]$, we only take into account the memory impacts of ξ_1 and not at the beginning at ξ_0; the revised FDE reads as follows ${}_{\xi_1}^{c}\mathbb{D}_{\xi}^{\varphi_1}\mathbf{x} = \mathbf{g}(\mathbf{x}, \xi)$ supplemented by $\mathbf{x}(\xi_1) = \mathbf{x}_1$. The initial setting $(\xi_1, \mathbf{x}_1)$ now demands the fractional-order to be fluctuated by φ_1. Here, we apply $\mathbf{x}_1 = \mathbf{x}(\xi_1^-)$; as the solution of ${}_{\xi_0}^{c}\mathbb{D}_{\xi}^{\varphi_0}\mathbf{x} = \mathbf{g}(\mathbf{x}, \xi)$. Furthermore, we gradually develop a fixed memory scheme over the range $[\xi_0, \mathbb{T}]$.

3.2. Short-memory wind turbine aerodynamic model

Messadi et al. [4] proposed the wind turbine system with a PMSG in 2015. The PMSG is a quintessential slightly elevated dynamical, multivariate coupled system and when the input shaft has an impact field, it is extremely responsive to stack perturbations and contact pressure, and the variability of its specifications is recommended by the modelling of FC [46]. We proposed a wind turbine system with a PMSG through the use of a fractional derivatives, as follows:

$$\begin{cases} {}_{0}^{c}\mathbb{D}_{\xi}^{\mathbf{q}_1}\mathbf{x} = \delta_1(\mathbf{y} - \mathbf{x}) + \delta_2\mathbf{y}\mathbf{z}, \\ {}_{0}^{c}\mathbb{D}_{\xi}^{\mathbf{q}_2}\mathbf{y} = \delta_3\mathbf{x} - \mathbf{x}\mathbf{z} - \mathbf{y}, \\ {}_{0}^{c}\mathbb{D}_{\xi}^{\mathbf{q}_3}\mathbf{z} = \mathbf{x}\mathbf{y} - \mathbf{z}, \end{cases} \tag{3.10}$$

where $q_{\wp} \in (0,1),\ \wp = 1, ..., 3$ are dimension-free terms and $\delta_1 = 5.45, \delta_2 = 1$ and $\delta_3 = 20$ are operating parameters.

3.3. Qualitative analysis of the FO wind turbine model

Addressing the FO wind turbine corresponding to (3.10) will reveal its equilibria by substituting the left-hand side of (3.10) with zero.

$$\begin{cases} 0 = \delta_1(\mathbf{y} - \mathbf{x}) + \delta_2 \mathbf{yz}, \\ 0 = \delta_3 \mathbf{x} - \mathbf{xz} - \mathbf{y}, \\ 0 = \mathbf{xy} - \mathbf{z}. \end{cases} \tag{3.11}$$

The three equilibria points of model (3.10) are $\mathcal{E}_1 = (0,0,0)$ and $\mathcal{E}_{2,3} = (\mathbf{y} - 1, \pm\sqrt{\mathbf{y} - 1}, \pm\sqrt{\mathbf{y} - 1})$. And the Jacobian matrix is specified as

$$\mathcal{J} = \begin{pmatrix} -\delta_1 & \delta_1 + \delta_2 \mathbf{z} & \delta_2 \mathbf{y} \\ -\mathbf{z} + \delta_3 & -1 & -\mathbf{x} \\ \mathbf{y} & \mathbf{x} & -1 \end{pmatrix} \tag{3.12}$$

where $\mathbf{x}, \mathbf{y}$ and $\mathbf{z}$ denote the equilibrium points.

Furthermore, (2.2) presents the Lyapunov exponents as $\bar{L}_1 = 0.852023, \bar{L}_2 = 0.009746$ and $\bar{L}_1 = 8.502219$. Figure 2 displays the simulation's numerical outcomes.

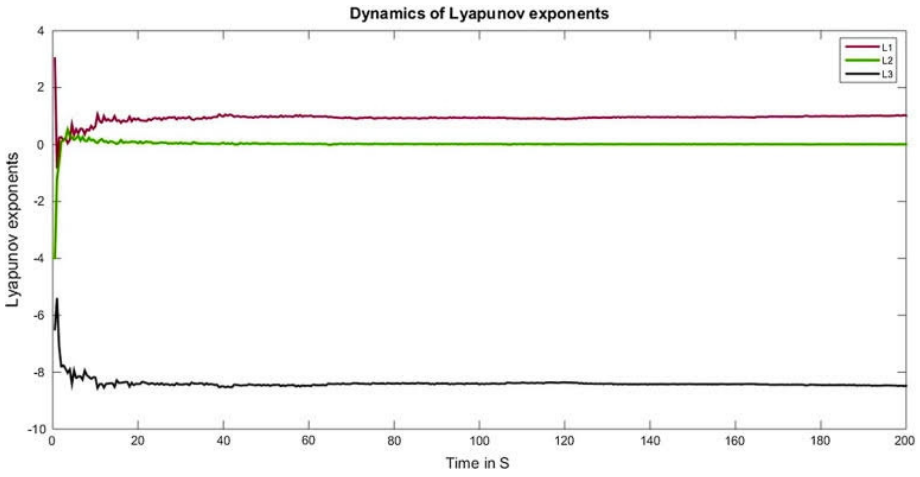

Figure 2. Plot of Lyapunov exponents.

Theorem 3.1. *Suppose that* $\lambda > 0,\ \eta > 0,\ \delta_1 > 0, \delta_2$ *and* $\delta_3 > 0$ *with*

$$\mho_{\lambda,\eta} = \left\{(\mathbf{x}, \mathbf{y}, \mathbf{z}) | \lambda \mathbf{x}^2 + (\lambda + \eta)\mathbf{y}^2 + \eta\Big[\mathbf{z} - \frac{(\delta_1 + \delta_3)\lambda + \eta\delta_3}{\eta}\Big]^2\right\} \leq \mathbb{R}^2_{\lambda,\eta}, \tag{3.13}$$

where

$$\mathbb{R}^2_{\lambda,\eta} = \begin{cases} \frac{\delta_2^2}{4\delta_1(\delta_2 - \delta_1)} \frac{((\delta_1+\delta_3)\lambda+\eta\delta_3)^2}{\eta}, & \delta_1 \geq 1, \delta_2 \geq 2\delta_1, \\ \frac{\delta_2^2}{4(\delta_2 - 1)} \frac{((\delta_1+\delta_3)\lambda+\eta\delta_3)^2}{\eta}, & \delta_1 > 1, \delta_2 \geq 2, \\ ((\delta_1 + \delta_3)\lambda + \eta\delta_3)^2, & \delta_2 < 2\delta_1,\ \delta_2 < 2. \end{cases} \tag{3.14}$$

Then, $\mho_{\lambda,\eta}$ is the ultimate bound and positively invariant set of model (3.10).

Proof. Introducing the Lyapunov-type candidate gives

$$\begin{aligned}\mathcal{U}_{\lambda,\eta}(\mathbf{U}) &= \mathcal{U}_{\lambda,\eta}(\mathbf{x},\mathbf{y},\mathbf{z})\\ &= \lambda\mathbf{x}^2+(\lambda+\eta)\mathbf{y}^2+\eta\Big[\mathbf{z}-\frac{(\delta_1+\delta_3)\lambda+\eta\delta_3}{\eta}\Big]^2,\ \ \forall\ \lambda,\eta>0.\end{aligned}\tag{3.15}$$

Then, the derivative of $\mathcal{U}_{\lambda,\eta}(\mathbf{U})$ is

$$\begin{aligned}\dot{\mathcal{U}}_{\lambda,\eta}(\mathbf{U}) &= 2\lambda\mathbf{x}\dot{\mathbf{x}}+2(\lambda+\eta)\mathbf{y}\dot{\mathbf{y}}+2\eta\Big[\mathbf{z}-\frac{(\delta_1+\delta_3)\lambda+\eta\delta_3}{\eta}\Big]\dot{\mathbf{z}}\\ &= 2\lambda\mathbf{x}(\delta_1\mathbf{y}-\delta_1\mathbf{x}+\delta_2\mathbf{y}\mathbf{z})+2(\eta+\lambda)\mathbf{y}(\delta_3\mathbf{x}-\mathbf{y}-\mathbf{x}\mathbf{z})+2\eta\Big[\mathbf{z}-\frac{(\delta_1+\delta_3)\lambda+\eta\delta_3}{\eta}\Big](\mathbf{x}\mathbf{y}-\mathbf{z})\\ &= -2\delta_1\lambda\mathbf{x}^2-2(\eta+\lambda)\mathbf{y}^2-2\eta\delta_2\mathbf{z}^2+2\delta_2\big((\delta_1+\delta_3)\lambda+\eta\delta_3\big)\mathbf{z}.\end{aligned}\tag{3.16}$$

Assume that $\dot{\mathcal{U}}_{\lambda,\eta}(\mathbf{U})=0$ and we attain a bounded closed set Θ :

$$\Theta=\left\{(\mathbf{x},\mathbf{y},\mathbf{z})\Big|\frac{4\delta_1\eta\lambda\mathbf{x}^2}{\delta_2[(\delta_1+\delta_3)\lambda+\eta\delta_3]^2}+\frac{4\eta(\eta+\lambda)\mathbf{y}^2}{\delta_2[(\delta_1+\delta_3)\lambda+\eta\delta_3]^2}+\frac{4\eta^2[\mathbf{z}-((\delta_1+\delta_3)\lambda+\eta\delta_3)/2\eta]^2}{[(\delta_1+\delta_3)\lambda+\eta\delta_3]^2}=1\right\}.\tag{3.17}$$

Because the chaotic framework given by (3.10) is bounded, the continuous function given by (3.15) is able to attain its greatest value on the above-mentioned bounded closed set.

As a result, solutions to the structure described by (3.10) exist in the set defined by $\{(\mathbf{x},\mathbf{y},\mathbf{z})\big|\mathcal{U}_{\lambda,\eta}(\mathbf{U})\le\max\mathcal{U}_{\lambda,\eta}(\mathbf{U})=\mathbb{R}^2_{\lambda,\eta},\mathbf{U}\in\Theta\}$. By solving the constrained extremum problem that follows, we can achieve the maximum value of function (3.15) as follows:

$$\max\ \mathcal{U}_{\lambda,\eta}(\mathbf{U})=\max\left\{\lambda\mathbf{x}^2+(\lambda+\eta)\mathbf{y}^2+\eta\Big[\mathbf{z}-\frac{(\delta_1+\delta_3)\lambda+\eta\delta_3}{\eta}\Big]^2\right\}\tag{3.18}$$

such that

$$\frac{4\delta_1\eta\lambda\mathbf{x}^2}{\delta_2[(\delta_1+\delta_3)\lambda+\eta\delta_3]^2}+\frac{4\eta(\eta+\lambda)\mathbf{y}^2}{\delta_2[(\delta_1+\delta_3)\lambda+\eta\delta_3]^2}+\frac{4\eta^2[\mathbf{z}-((\delta_1+\delta_3)\lambda+\eta\delta_3)/2\eta]^2}{[(\delta_1+\delta_3)\lambda+\eta\delta_3]^2}=1.\tag{3.19}$$

Letting $\mathbf{x}_1=\sqrt{\lambda}\mathbf{x}$, $\mathbf{y}_1=\sqrt{\eta+\lambda}\mathbf{y}$, $\mathbf{z}_1=\sqrt{\eta}\mathbf{z}$, $\gamma=\frac{(\delta_1+\delta_3)\lambda+\eta\delta_3}{2\sqrt{\eta}}$, $\alpha^2=\frac{\delta_2[(\delta_1+\delta_3)\lambda+\eta\delta_3]^2}{4\eta\delta_1}$ *and* $\mathfrak{I}^2=\frac{\delta_2[(\delta_1+\delta_3)\lambda+\eta\delta_3]^2}{4\eta}$, then (3.19) reduces to the subsequent form: $\max\ \mathcal{U}_{\lambda,\eta}(\mathbf{U})=\max\{\mathbf{x}_1^2+\mathbf{y}_1^2+(\mathbf{z}_1-2\gamma)^2\}$ such that

$$\frac{\mathbf{x}_1^2}{\alpha^2}+\frac{\mathbf{y}_1^2}{\mathfrak{I}^2}+\frac{(\mathbf{z}_1-\gamma)^2}{\gamma^2}=1.\tag{3.20}$$

We can address (3.20) using the optimisation approach and obtain the formula $\mathbb{R}^2_{\lambda,\eta}$ as follows:

$$\mathbb{R}^2_{\lambda,\eta}=\begin{cases}\frac{\delta_2^2}{4\delta_1(\delta_2-\delta_1)}\frac{((\delta_1+\delta_3)\lambda+\eta\delta_3)^2}{\eta}, & \delta_1\ge1,\delta_2\ge2\delta_1,\\ \frac{\delta_2^2}{4(\delta_2-1)}\frac{((\delta_1+\delta_3)\lambda+\eta\delta_3)^2}{\eta}, & \delta_1>1,\delta_2\ge2,\\ ((\delta_1+\delta_3)\lambda+\eta\delta_3)^2, & \delta_2<2\delta_1,\ \delta_2<2.\end{cases}\tag{3.21}$$

This completes the proof.

Remark 3.1. Assume that $\eta = 1$ and $\lambda = 1$; then, Theorem 3.1 reduces to

$$\mho_{1,1} = \left\{(\mathbf{x}, \mathbf{y}, \mathbf{z}) \middle| \mathbf{x}^2 + 2\mathbf{y}^2 + (\mathbf{z} - \delta_1 - 2\delta_3)^2 \leq F^2\right\} \tag{3.22}$$

as the ultimate bound and positively invariant set of (3.11), where

$$\mathbb{R}^2_{\lambda,\eta} = \begin{cases} \frac{\delta_2^2(\delta_1+2\delta_3)^2}{4\delta_1(\delta_2-\delta_1)}, & \delta_1 \geq 1, \delta_2 \geq 2\delta_1, \\ \frac{\delta_2^2(\delta_1+2\delta_3)^2}{4(\delta_2-1)}, & \delta_1 > 1, \delta_2 \geq 2, \\ (\delta_1 + 2\delta_3)^2, & \delta_2 < 2\delta_1,\ \delta_2 < 2. \end{cases}$$

Consider the non-negative specific values $\delta_1 = 35,\ \delta_2 = 7$ and $\delta_3 = 25$ in $\mho_{1,1}$ above; then, we are able to determine that

$$\mho_{1,1} = \left\{(\mathbf{x}, \mathbf{y}, \mathbf{z}) \middle| \mathbf{x}^2 + 2\mathbf{y}^2 + (\mathbf{z} - 20.25)^2 \leq (121.45)^2\right\} \tag{3.23}$$

is the ultimate bound and positively invariant set for model (3.10).

Now, we propose a novel short-memory wind turbine system with a PMSG described as follows:

$$\begin{cases} {}^{c}_{\xi^*}\mathbb{D}^{\mathbf{q}_1}_{\xi}\mathbf{x} = \delta_1(\mathbf{y} - \mathbf{x}) + \delta_2\mathbf{y}\mathbf{z}, \\ {}^{c}_{\xi^*}\mathbb{D}^{\mathbf{q}_2}_{\xi}\mathbf{y} = \delta_3\mathbf{x} - \mathbf{x}\mathbf{z} - \mathbf{y}, \\ {}^{c}_{\xi^*}\mathbb{D}^{\mathbf{q}_3}_{\xi}\mathbf{z} = \mathbf{x}\mathbf{y} - \mathbf{z}, \end{cases} \tag{3.24}$$

supplemented with the ICs $\mathbf{x}(0) = \mathbf{x}_0,\ \mathbf{y}(0) = \mathbf{y}_0$ and $\mathbf{z}(0) = \mathbf{z}_0$.

The specifications and order of the framework are changed, and the bifurcation schemes for framework (3.10) are resolved at $\delta_2 = 20$ and $\delta_1 = 15.46$. By correlating the eigenvalues and Lyapunov exponents and incorporating the FO bifurcation plots, it is possible to see that the chaotic behaviour of the framework exhibits broader Lyapunov exponents as the order of the fractional equation remains between $\mathbf{q} \in [0.6, 0.9]$. Therefore, FO restrictions for chaos reduction are more effective than classical control.

Due to the fact that nonlinear processes have multiple equilibria, they have much more complicated stability approaches than FO linearization. This matter is still unresolved [47]. The examples that follow show plenty of outcomes.

Theorem 3.2. *The equilibria are asymptotically stable for* $\mathbf{q}_1 = \mathbf{q}_2 = \mathbf{q}_3 = \mathbf{q}$ *if all of the eigenvalues* $\Xi_\wp$ $(\wp = 1, 2, 3)$ *of the Jacobian matrix* $\mathbb{J} = \frac{\partial \mathbf{g}}{\partial \mathbf{x}}$, *where* $\mathbf{g} = [\mathbf{g}_1, \mathbf{g}_2, \mathbf{g}_3]^{\mathcal{T}}$, *elaborated at the equilibrium* $\mathcal{E}^*$, *are subject to the subsequent criterion:*

$$\left|\arg(eig\mathbb{J})\right| = |\arg(\Xi_\wp)| > \frac{\mathbf{q}\pi}{2},\ \ \wp = 1, 2, 3. \tag{3.25}$$

When we consider the incommensurate FO system $\mathbf{q}_1 \neq \mathbf{q}_2 \neq \mathbf{q}_3$ *and suppose that* $\mathfrak{m}$ *is the least common multiple of the denominators* $\mathbf{u}_\wp$*'s of* $\mathbf{q}_\wp$*'s, where* $\mathbf{q}_\wp = \mathbf{v}_\wp/\mathbf{u}_\wp,\ \mathbf{v}_\wp, \mathbf{u}_\wp \in \mathbb{Z}^+$ *for* $\wp = 1, 2, 3$, *and adjusting* $\varsigma = 1/\mathfrak{m}$, *which indicates that* (3.10) *is asymptotically stable if* $|\arg(\Xi)| > \frac{\varsigma\pi}{2}$ *for all roots* Ξ *of the following equation:*

$$\det(diag([\Xi^{\varsigma\mathbf{q}_1}\ \Xi^{\varsigma\mathbf{q}_2}\ \Xi^{\varsigma\mathbf{q}_3}]) - \mathbb{J}) = 0. \tag{3.26}$$

A necessary stability condition for FO systems (3.10) *to remain chaotic is keeping at least one eigenvalue* Ξ *in the unstable region [48]. A previous summary [49] precisely outlined the handful of equilibria and eigenvalues for one-scroll, double-scroll, and multiscroll attractors. Consider the scenario where there are only three equilibria in a three-dimensional dynamic scheme. As a result, a structure with a double-scroll attractor might have two saddle-focus points that are encircled by scrolls, one more saddle point, etc. We should evaluate the characteristic equations for the linear parts with slopes* **c** *and* **d***, respectively, in the particular instance of the piecewise nonlinearity shown in Figure 3.*

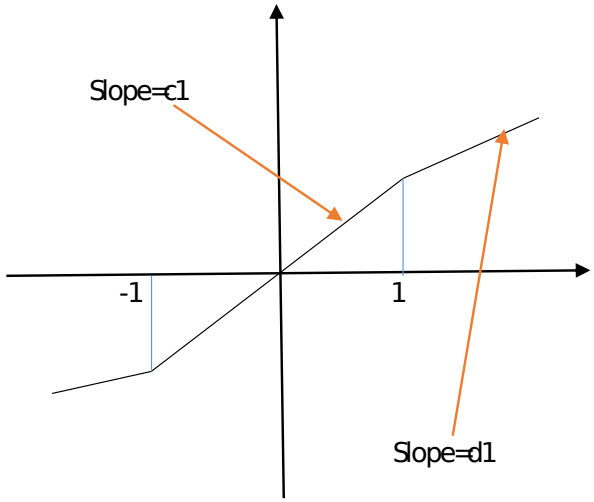

Figure 3. A piecewise-linear flux-controlled memristor's features.

Maintaining one or more eigenvalues in the unstable eigenvalues of scroll saddle points $\Xi_{1,2} = \bar{r}_{1,2} \pm \jmath\omega_{1,2}$. *These are the necessary conditions to exhibit the double-scroll attractor of* (3.10) *is the eigenvalues* $\Xi_{1,2}$ *remaining in the unstable region. We can also establish a minimal order* $\mathbf{q}$ *for which a dynamical framework exhibits chaotic behaviour in accordance with condition* $\mathbf{q} > \frac{2}{\pi} arctan\left(\frac{|\omega_\wp|}{\bar{r}_\wp}\right)$, $\wp = 1, 2$.

4. Numerical schemes

Here, we present several schemes for the solution of a wind turbine system with a PMSG.

4.1. Piecewise fractional derivative scheme

Assume that $\xi^* = \mathbb{T}_\kappa$, $\kappa \in [0, \mathfrak{m}]$ *and* $[0, \mathbb{T}] = [\mathbb{T}_0, \mathbb{T}_1] \cup (\mathbb{T}_1, \mathbb{T}_2] \cup, ..., \cup (\mathbb{T}_\mathfrak{m}, \mathbb{T}_{\mathfrak{m}+1} = \mathbb{T}]$. Furthermore, ξ^* starts form $\mathbb{T}_0$. For $\xi \in (\mathbb{T}_{\kappa-1}, \mathbb{T}]$, the framework (3.24) is only dependent upon the state starting at time $\xi^* = \mathbb{T}_{\kappa-1}$, often not starting at time $\xi^* = 0$, as is the case for (3.24). Additionally, the FO $\mathbf{q}_\wp$ on every sub-interval is a crucial factor to characterise memory consequences and it may fluctuate. Furthermore, a piecewise mapping $\mathbf{q}_\wp$ is stated by $\mathbf{q}_\wp(\xi) = \mathbf{q}_{\wp,\kappa}$, $\xi \in (\mathbb{T}_{\kappa-1}, \mathbb{T}_\kappa]$, $\wp = 1, 2, 3$. $\mathbf{q}_{\wp,\kappa}$ represents a constant and $\mathbf{q}_{\wp,\kappa} \in (0, 1]$. Thus, we can obtain every sub-system one by one.

For $\xi \in (0, \mathbb{T}_1]$ and $(\mathbf{x}_0, \mathbf{y}_0, \mathbf{z}_0)$, we have

$$\begin{cases} {}_0^c\mathbb{D}_\xi^{\mathbf{q}_1,0}\mathbf{x} = \delta_1(\mathbf{y}-\mathbf{x}) + \delta_2\mathbf{y}\mathbf{z}, \\ {}_0^c\mathbb{D}_\xi^{\mathbf{q}_2,0}\mathbf{y} = \delta_3\mathbf{x} - \mathbf{x}\mathbf{z} - \mathbf{y}, \\ {}_0^c\mathbb{D}_\xi^{\mathbf{q}_3,0}\mathbf{z} = \mathbf{x}\mathbf{y} - \mathbf{z}. \end{cases} \tag{4.1}$$

For $\xi \in (\mathbb{T}_1, \mathbb{T}_2]$, numerical techniques can be used to acquire the situation $\mathbf{x}(\mathbb{T}_1)$ from (3.24) as the revised ICs of

$$\begin{cases} {}_{\mathbb{T}_1}^c\mathbb{D}_\xi^{\mathbf{q}_1,1}\mathbf{x} = \delta_1(\mathbf{y}-\mathbf{x}) + \delta_2\mathbf{y}\mathbf{z}, \\ {}_{\mathbb{T}_1}^c\mathbb{D}_\xi^{\mathbf{q}_2,1}\mathbf{y} = \delta_3\mathbf{x} - \mathbf{x}\mathbf{z} - \mathbf{y}, \\ {}_{\mathbb{T}_1}^c\mathbb{D}_\xi^{\mathbf{q}_3,1}\mathbf{z} = \mathbf{x}\mathbf{y} - \mathbf{z}. \end{cases} \tag{4.2}$$

$$\vdots .$$

For $\xi \in (\mathbb{T}_\mathfrak{m}, \mathbb{T}]$, numerical techniques can be used to acquire the situation $\mathbf{x}(\mathbb{T}_\mathfrak{m})$; then, we have

$$\begin{cases} {}_{\mathbb{T}_\mathfrak{m}}^c\mathbb{D}_\xi^{\mathbf{q}_1,\mathfrak{m}}\mathbf{x} = \delta_1(\mathbf{y}-\mathbf{x}) + \delta_2\mathbf{y}\mathbf{z}, \\ {}_{\mathbb{T}_\mathfrak{m}}^c\mathbb{D}_\xi^{\mathbf{q}_2,\mathfrak{m}}\mathbf{y} = \delta_3\mathbf{x} - \mathbf{x}\mathbf{z} - \mathbf{y}, \\ {}_{\mathbb{T}_\mathfrak{m}}^c\mathbb{D}_\xi^{\mathbf{q}_3,\mathfrak{m}}\mathbf{z} = \mathbf{x}\mathbf{y} - \mathbf{z}. \end{cases} \tag{4.3}$$

4.2. Discrete fractional derivative scheme

Throughout this investigation, we consider that $\ell = \mathbf{q}_{1,\kappa} = \mathbf{q}_{2,\kappa} = \mathbf{q}_{3,\kappa}$. Our aim is to demonstrate the chaotic behaviour on every sub-region. We employ the accurate discretisation by the fractional derivative on the time scale [36] to prevent uncertainties. We suggest the discrete-time system (3.24) analogue shown below:

$$\begin{cases} {}^c\nabla^\ell_{\xi^*,\hbar}\mathbf{x} = \delta_1(\mathbf{y}(\xi+(\ell-1)\hbar) - \mathbf{x}(\xi+(\ell-1)\hbar)) + \delta_2\mathbf{y}(\xi+(\ell-1)\hbar)\mathbf{z}(\xi+(\ell-1)\hbar), \\ {}^c\nabla^\ell_{\xi^*,\hbar}\mathbf{y} = \delta_3\mathbf{x}(\xi+(\ell-1)\hbar) - \mathbf{x}(\xi+(\ell-1)\hbar)\mathbf{z}(\xi+(\ell-1)\hbar) - \mathbf{y}(\xi+(\ell-1)\hbar), \\ {}^c\nabla^\ell_{\xi^*,\hbar}\mathbf{z} = \mathbf{x}(\xi+(\ell-1)\hbar)\mathbf{y}(\xi+(\ell-1)\hbar) - \mathbf{z}(\xi+(\ell-1)\hbar, \end{cases} \tag{4.4}$$

where $\ell \in (0, 1]$ and $\xi, \xi^* \in \mathbb{N}_{\mathbf{a}+(1-\ell)\hbar}$.

Assume that there is a nonnegative integer ϖ, $\mathbb{T}_\kappa = \mathbf{a} + \kappa\hbar$ and ℓ signifies the piecewise constant mapping stated by

$$\ell = \begin{cases} \ell_0, \ \xi \in \{\mathbf{a}, \mathbf{a}+\hbar, ..., \mathbf{a}+\varpi\hbar\}; \\ \ell_1, \ \xi \in \{\mathbf{a}+\varpi\hbar+\hbar, ..., \mathbf{a}+2\varpi\hbar\}; \\ \vdots \\ \ell_\mathfrak{m}, \ \xi \in \{\mathbf{a}+\mathfrak{m}\hbar+\hbar, ..., \mathbf{a}+(\mathfrak{m}+1)\varpi\hbar\}. \end{cases} \tag{4.5}$$

For $\mathfrak{n} \in \{0, ..., \varpi - 1\}$, we have

$$\begin{cases} \mathbf{x}_{\mathfrak{n}+1} = \mathbf{x}_0 + \frac{\hbar^{\ell_0}}{\Gamma(\ell_0)} \sum\limits_{J=0}^{\mathfrak{n}} \frac{\Gamma(\mathfrak{n}-J+\ell_0)}{\Gamma(\mathfrak{n}-J+1)} \Big\{\delta_1(\mathbf{y}_J - \mathbf{x}_J) + \delta_2 \mathbf{y}_J \mathbf{z}_J\Big\}, \\ \mathbf{y}_{\mathfrak{n}+1} = \mathbf{y}_0 + \frac{\hbar^{\ell_0}}{\Gamma(\ell_0)} \sum\limits_{J=0}^{\mathfrak{n}} \frac{\Gamma(\mathfrak{n}-J+\ell_0)}{\Gamma(\mathfrak{n}-J+1)} \Big\{\delta_3 \mathbf{x}_J - \mathbf{x}_J \mathbf{z}_J - \mathbf{y}_J\Big\}, \\ \mathbf{z}_{\mathfrak{n}+1} = \mathbf{z}_0 + \frac{\hbar^{\ell_0}}{\Gamma(\ell_0)} \sum\limits_{J=0}^{\mathfrak{n}} \frac{\Gamma(\mathfrak{n}-J+\ell_0)}{\Gamma(\mathfrak{n}-J+1)} \Big\{\mathbf{x}_J \mathbf{y}_J - \mathbf{z}_J\Big\}. \end{cases} \tag{4.6}$$

For $\mathfrak{n} \in \{\varpi, ..., 2\varpi - 1\}$, we have

$$\begin{cases} \mathbf{x}_{\mathfrak{n}+1} = \mathbf{x}_\varpi + \frac{\hbar^{\ell_1}}{\Gamma(\ell_1)} \sum\limits_{J=0}^{\mathfrak{n}} \frac{\Gamma(\mathfrak{n}-J+\ell_1)}{\Gamma(\mathfrak{n}-J+1)} \Big\{\delta_1(\mathbf{y}_J - \mathbf{x}_J) + \delta_2 \mathbf{y}_J \mathbf{z}_J\Big\}, \\ \mathbf{y}_{\mathfrak{n}+1} = \mathbf{y}_\varpi + \frac{\hbar^{\ell_1}}{\Gamma(\ell_1)} \sum\limits_{J=0}^{\mathfrak{n}} \frac{\Gamma(\mathfrak{n}-J+\ell_1)}{\Gamma(\mathfrak{n}-J+1)} \Big\{\delta_3 \mathbf{x}_J - \mathbf{x}_J \mathbf{z}_J - \mathbf{y}_J\Big\}, \\ \mathbf{z}_{\mathfrak{n}+1} = \mathbf{z}_\varpi + \frac{\hbar^{\ell_1}}{\Gamma(\ell_1)} \sum\limits_{J=0}^{\mathfrak{n}} \frac{\Gamma(\mathfrak{n}-J+\ell_1)}{\Gamma(\mathfrak{n}-J+1)} \Big\{\mathbf{x}_J \mathbf{y}_J - \mathbf{z}_J\Big\}. \end{cases} \tag{4.7}$$

$$\vdots .$$

Furthermore, let us note the complexities on $[\mathbb{T}_0, \mathbb{T}_1], ..., (\mathbb{T}_2, \mathbb{T}_3]$, where $\mathbb{T}_0 = \mathbf{a} = 0$ and $\mathbb{T}_\kappa \in \{\mathbf{a}, \mathbf{a} + \hbar, ...\}$. The data are expressed by $\hbar$ and the value of ℓ_κ has a significant impact on the system's state, as described by (4.4). The interactions of variable-order are often incredibly complex. The wind turbine system (4.4) with a PMSG has a wide energetic range. To distinguish between chaotic regions, we compute the Lyapunov exponents using the Jacobian matrix method [50].

Initially, the first sub-interval of the framework (4.4) can be configured as

$$\begin{cases} \mathbf{x}_{\mathfrak{n}+1} = \mathbf{x}_0 + \frac{\hbar^{\ell}}{\Gamma(\ell)} \sum\limits_{J=0}^{\mathfrak{n}} \frac{\Gamma(\mathfrak{n}-J+\ell)}{\Gamma(\mathfrak{n}-J+1)} \Big\{\delta_1(\mathbf{y}_J - \mathbf{x}_J) + \delta_2 \mathbf{y}_J \mathbf{z}_J\Big\}, \\ \mathbf{y}_{\mathfrak{n}+1} = \mathbf{y}_0 + \frac{\hbar^{\ell}}{\Gamma(\ell)} \sum\limits_{J=0}^{\mathfrak{n}} \frac{\Gamma(\mathfrak{n}-J+\ell)}{\Gamma(\mathfrak{n}-J+1)} \Big\{\delta_3 \mathbf{x}_J - \mathbf{x}_J \mathbf{z}_J - \mathbf{y}_J\Big\}, \\ \mathbf{z}_{\mathfrak{n}+1} = \mathbf{z}_0 + \frac{\hbar^{\ell}}{\Gamma(\ell)} \sum\limits_{J=0}^{\mathfrak{n}} \frac{\Gamma(\mathfrak{n}-J+\ell)}{\Gamma(\mathfrak{n}-J+1)} \Big\{\mathbf{x}_J \mathbf{y}_J - \mathbf{z}_J\Big\}. \end{cases} \tag{4.8}$$

The Jacobian matrix for the system (4.4) can be presented as

$$\mathbb{J}(\mathfrak{n}) = \begin{pmatrix} a_{11}(\mathfrak{n}) & a_{12}(\mathfrak{n}) & a_{13}(\mathfrak{n}) \\ b_{21}(\mathfrak{n}) & b_{22}(\mathfrak{n}) & b_{23}(\mathfrak{n}) \\ c_{31}(\mathfrak{n}) & c_{32}(\mathfrak{n}) & c_{33}(\mathfrak{n}) \end{pmatrix}, \tag{4.9}$$

where $a_{11}(\mathfrak{n}) = b_{22}(\mathfrak{n}) = c_{33}(\mathfrak{n}) = 1$ and $\mathbb{J} = \mathcal{I}$ denotes an identity matrix.

The framework of tangent maps can be defined for every component, as follows:

$$a_{11}(\mathfrak{n}+1) = a_{11}(0) + \frac{\hbar^{\ell}}{\Gamma(\ell)} \sum_{J=0}^{\mathfrak{n}} \frac{\Gamma(\mathfrak{n}-J+\ell)}{\Gamma(\mathfrak{n}-J+1)} [\delta_1(b_{21}(J) - a_{11}(J)) + \delta_2 b_{21}(J) c_{31}(J)],$$

$$a_{12}(\mathfrak{n}+1) = a_{12}(0) + \frac{\hbar^{\ell}}{\Gamma(\ell)}\sum_{\jmath=0}^{\mathfrak{n}}\frac{\Gamma(\mathfrak{n}-\jmath+\ell)}{\Gamma(\mathfrak{n}-\jmath+1)}[\delta_1(b_{22}(\jmath)-a_{12}(\jmath))+\delta_2 b_{22}(\jmath)c_{32}(\jmath)],$$

$$a_{13}(\mathfrak{n}+1) = a_{13}(0) + \frac{\hbar^{\ell}}{\Gamma(\ell)}\sum_{\jmath=0}^{\mathfrak{n}}\frac{\Gamma(\mathfrak{n}-\jmath+\ell)}{\Gamma(\mathfrak{n}-\jmath+1)}[\delta_1(b_{23}(\jmath)-a_{13}(\jmath))+\delta_2 b_{23}(\jmath)c_{33}(\jmath)],$$

$$b_{21}(\mathfrak{n}+1) = b_{21}(0) + \frac{\hbar^{\ell}}{\Gamma(\ell)}\sum_{\jmath=0}^{\mathfrak{n}}\frac{\Gamma(\mathfrak{n}-\jmath+\ell)}{\Gamma(\mathfrak{n}-\jmath+1)}[\delta_3 a_{11}(\jmath)-a_{11}(\jmath)c_{31}(\jmath)-b_{21}(\jmath)],$$

$$b_{22}(\mathfrak{n}+1) = b_{22}(0) + \frac{\hbar^{\ell}}{\Gamma(\ell)}\sum_{\jmath=0}^{\mathfrak{n}}\frac{\Gamma(\mathfrak{n}-\jmath+\ell)}{\Gamma(\mathfrak{n}-\jmath+1)}[\delta_3 a_{12}(\jmath)-a_{12}(\jmath)c_{32}(\jmath)-b_{22}(\jmath)],$$

$$b_{23}(\mathfrak{n}+1) = b_{23}(0) + \frac{\hbar^{\ell}}{\Gamma(\ell)}\sum_{\jmath=0}^{\mathfrak{n}}\frac{\Gamma(\mathfrak{n}-\jmath+\ell)}{\Gamma(\mathfrak{n}-\jmath+1)}[\delta_3 a_{13}(\jmath)-a_{13}(\jmath)c_{33}(\jmath)-b_{23}(\jmath)],$$

$$c_{31}(\mathfrak{n}+1) = c_{31}(0) + \frac{\hbar^{\ell}}{\Gamma(\ell)}\sum_{\jmath=0}^{\mathfrak{n}}\frac{\Gamma(\mathfrak{n}-\jmath+\ell)}{\Gamma(\mathfrak{n}-\jmath+1)}[a_{11}(\jmath)b_{21}(\jmath)-c_{31}(\jmath)],$$

$$c_{32}(\mathfrak{n}+1) = c_{32}(0) + \frac{\hbar^{\ell}}{\Gamma(\ell)}\sum_{\jmath=0}^{\mathfrak{n}}\frac{\Gamma(\mathfrak{n}-\jmath+\ell)}{\Gamma(\mathfrak{n}-\jmath+1)}[a_{12}(\jmath)b_{22}(\jmath)-c_{32}(\jmath)],$$

$$c_{33}(\mathfrak{n}+1) = c_{33}(0) + \frac{\hbar^{\ell}}{\Gamma(\ell)}\sum_{\jmath=0}^{\mathfrak{n}}\frac{\Gamma(\mathfrak{n}-\jmath+\ell)}{\Gamma(\mathfrak{n}-\jmath+1)}[a_{13}(\jmath)b_{23}(\jmath)-c_{33}(\jmath)]. \tag{4.10}$$

Then, all of the eigenvalues $\Xi_{\wp}(\mathfrak{n})$ of $\mathbb{J}(\mathfrak{n})$ are calculated using the singular value decomposition technique. Consequently, The approximate formula for the Lyapunov exponents spectrum is $\frac{\ln|\Xi_{\wp}(\mathfrak{n})|}{\mathfrak{n}}$, $\wp = 1, 2, 3$.

If there is a non-negative Lyapunov exponent, we can effectively use this technique to determine the chaotic regions for the second as well as other sub-intervals.

Suppose that $(\mathbf{x}_{\mathfrak{n}}, \mathbf{y}_{\mathfrak{n}}, \mathbf{z}_{\mathfrak{n}}) = (\mathbf{x}(\mathfrak{n}\hbar), \mathbf{y}(\mathfrak{n}\hbar), \mathbf{z}(\mathfrak{n}\hbar))$ along with the dynamical evaluation of the model (4.4). Assume that $\mathfrak{m} = 3, \hbar = 0.005$, $\mathbf{a} = 0.3$ and $\mathbf{b} = 0.8$. The initial settings are $\mathbf{x}_0 = 3, \mathbf{y}_0 = 3$ and $\mathbf{z}_0 = 3$ to analyse the dynamics on $[\mathbb{T}_0, \mathbb{T}_1], ..., (\mathbb{T}_2, \mathbb{T}_3]$, where $\mathbb{T}_0 = \mathbf{a} = 0$ and $\mathbb{T}_{\kappa} \in \{\mathbf{a}, \mathbf{a}+\hbar, ...\}$. The variable $\hbar$ is expressed and the value of ℓ has a significant impact on the system's state, as described by (4.4). The complexities of VO are often incredibly challenging. Memristors have a rich spectral response. According to Figure 4, varying φ_{κ} results in various chaotic attractors. But it is important to note that the ICs also influence the chaos $(\mathbf{x}_{\kappa\varpi}, \mathbf{y}_{\kappa\varpi}, \mathbf{z}_{\kappa\varpi})$. This implies that not every IC can produce chaos throughout all sub-intervals.

The adaptive nonlinear controllers of wind turbines with PMSG are being taken into account, and a proposed approach focused on a FO nonlinear control scheme is being explored. The d-axis flux is assumed to be zero to obtain the highest torque per ampere. As a result, the resonance frequency and the **q**-axis power flow will be related linearly. As infinite memory components are impossible to implement in MATLAB 2021 program, a finite truncation limit of 1000 is fixed to realize the FO system (4.4). Figure 5 depicts the PMSG model's configuration. To reach equilibrium at $\xi = 20$ seconds, the power flows $\iota_{\mathbf{q}_1}$ and $\iota_{\mathbf{d}}$, along with the angular velocity ω, were all monitored. The efficacy of the strategy described in this study is demonstrated by the similarity of the outcomes obtained with a fuzzified guaranteed cost controller [51]. Inferential controllers offer faster performance in the steady state than fuzzified controllers that meet the minimum requirements do. The presented fractional

dynamic converters are classified as speed loop controller algorithm frames in the control mechanism. Figure 6 depicts the velocity and power flow regulation with an unsettled interruption on the exterior. In Figure 7, the attractor bifurcation reactions are examined, and the orders $\mathbf{q}_1, \mathbf{q}_2$ and $\mathbf{q}_3$ are diversified. The bifurcation maps demonstrate how the FO significantly alters the structure's complexity.

The findings demonstrate the value of fractional calculus in dynamical electrical circuits. We obtain a strategy based on the framework that is smaller than the overall number of DEs while using FDEs. To suppress chaotic oscillations in a dynamic framework that is frequently defined by three equations, a control technique assumes that the operating parameters of the FO system are unknown even though chaos is still observable. The scenario is comparable to a hyperchaotic scheme. It expands the potential uses of the suggested chaotic mechanism. There is no doubt that the turbulent oscillations observed by Rajagopal et al. [52] are consistent with those corresponding to the existing methodology for discrete fractional operator and piecewise approaches. This further supports the validity of the ongoing project.

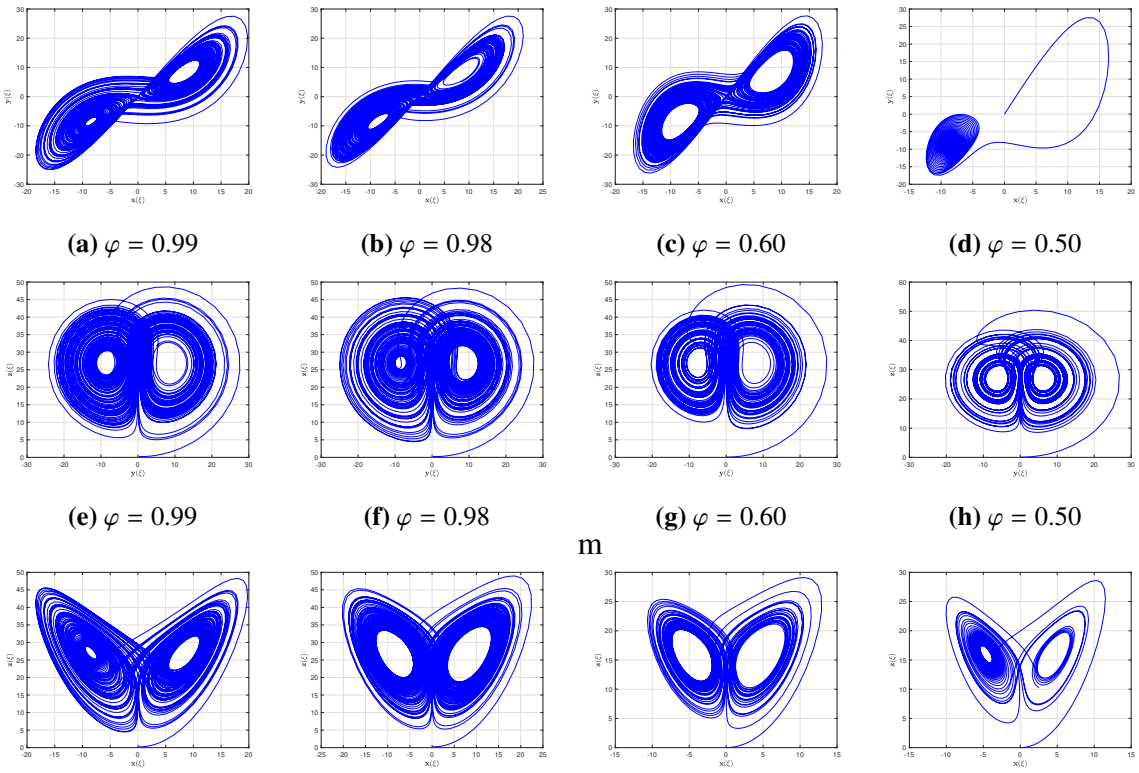

(a) $\varphi = 0.99$ **(b)** $\varphi = 0.98$ **(c)** $\varphi = 0.60$ **(d)** $\varphi = 0.50$

(e) $\varphi = 0.99$ **(f)** $\varphi = 0.98$ **(g)** $\varphi = 0.60$ **(h)** $\varphi = 0.50$

m

(i) $\varphi = 0.99$ **(j)** $\varphi = 0.98$ **(k)** $\varphi = 0.60$ **(l)** $\varphi = 0.50$

Figure 4. Graphical view of the chaos in the VO attractors given by model (4.4).

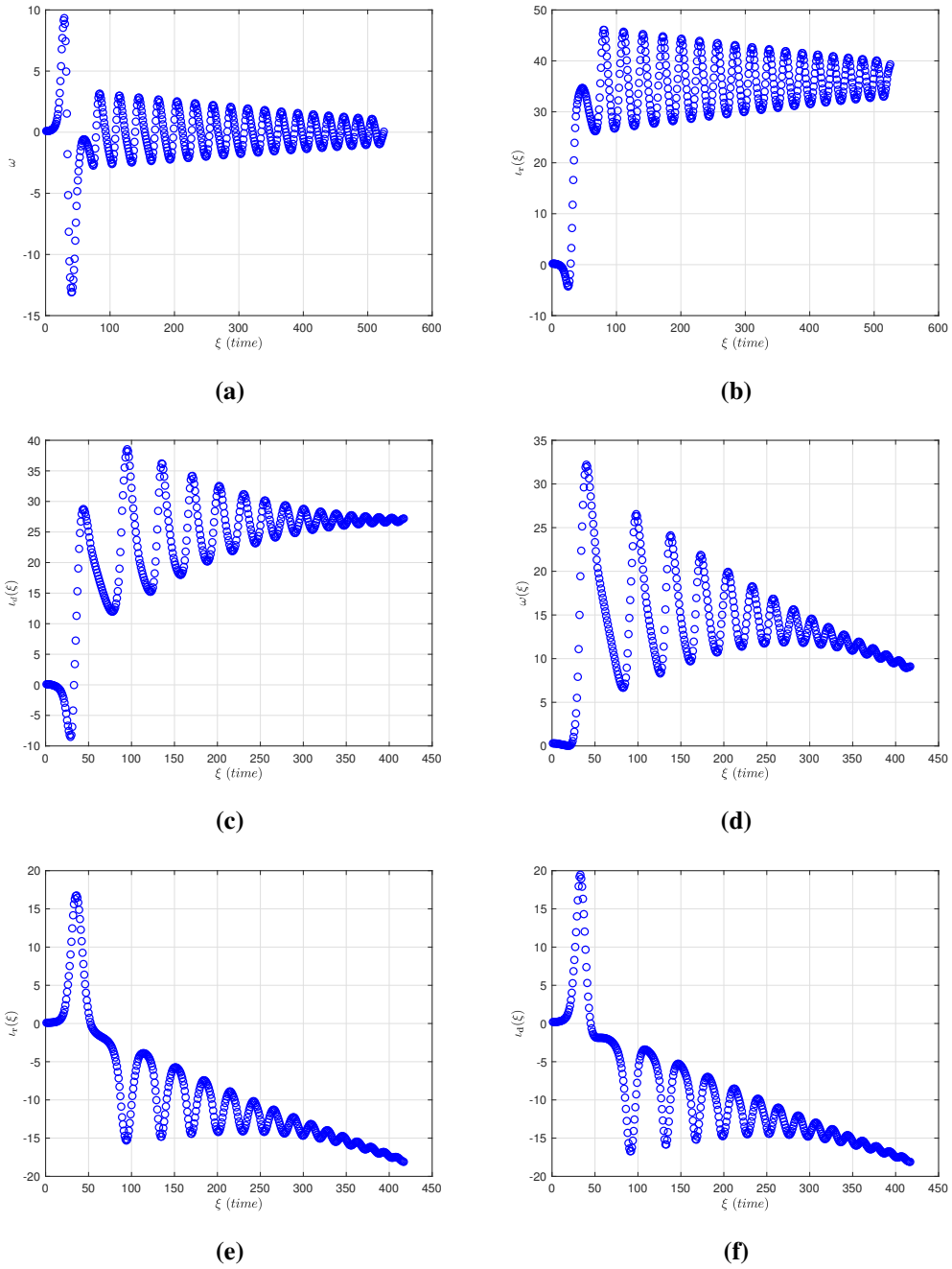

Figure 5. An adaptive learning system wherein guaranteed cost control was used to regulate the angular velocity of the PMSG to the steady state at time $\xi = 20$ seconds.

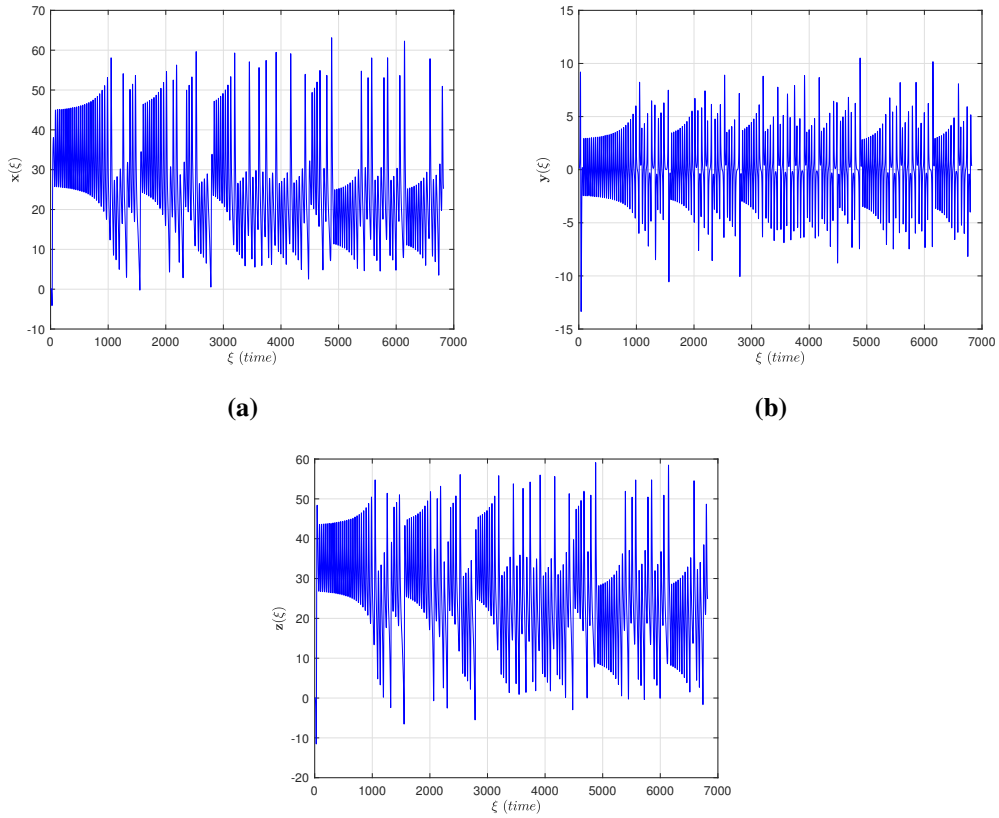

Figure 6. State variables of the quintessential chaotic attractor and the chaotic PMSG without influence when $\varphi = 0.95$.

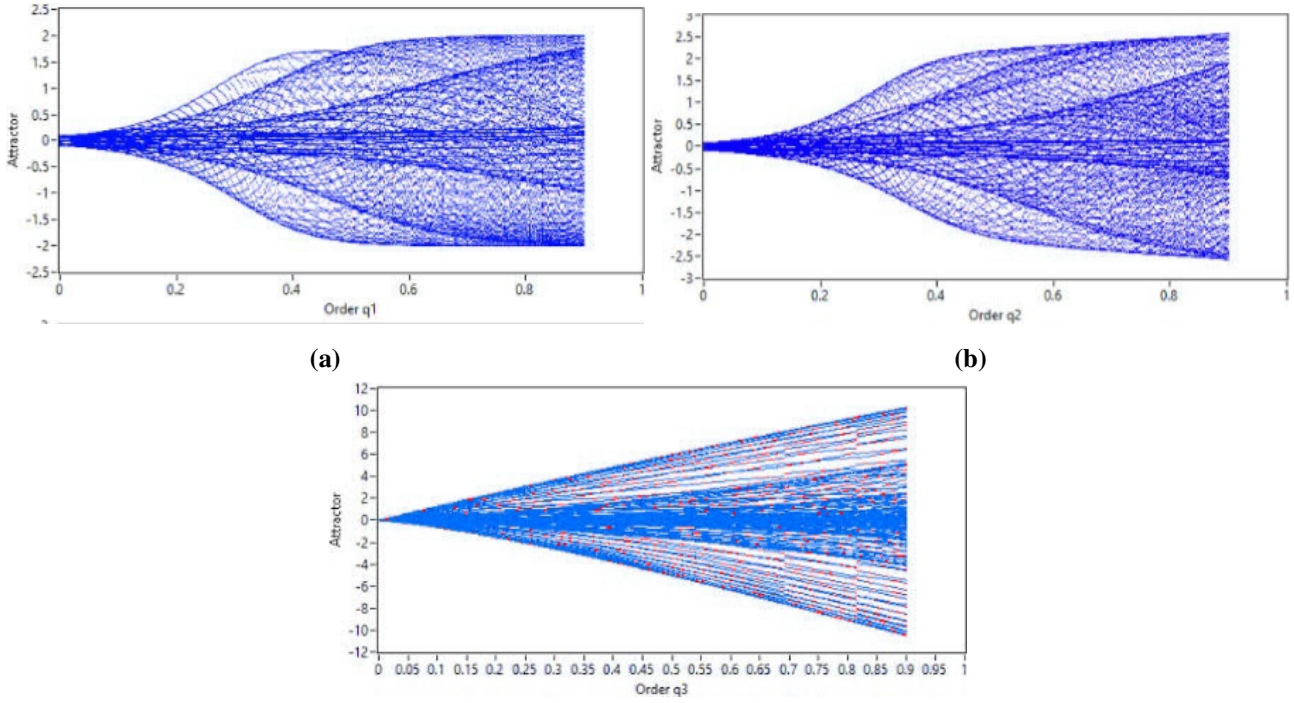

(a) **(b)**

(c)

Figure 7. Bifurcation states for $\mathbf{q}_1, \mathbf{q}_2$ and $\mathbf{q}_3$.

5. Conclusions

In this article, a short-memory framework for fractional modelling of a chaotic PMSG in a wind turbine system is presented. We provide explanations for innovative applications like the suppression of chaotic behaviour and physical meaning. Aside from that, piecewise components representing fractional VOs are also introduced. This report basically makes a significant contribution to the key segments by utilising the short-memory FDE mentioned above, a turbulent turbine configuration with a short memory is shown. The FO scheme and machine's Lyapunov exponents must be deduced in order to communicate the stability; thus, we used a novel technique to determine the expression of the Lyapunov first derivative. The PMSG framework and the suggested control strategies were incorporated into MATLAB for the available design experiments. The customised propellers' pitch angle and angular speed were calculated using dynamic programming, and predictive control was employed to monitor the calculated principles in a bid to garner the most influence. By applying the core principle of a numerical simulation of the tip speed ratio, pitch angle, drag coefficients, capacity factor, static pressure, and propeller angular velocity, the function of turbulent perturbations has been described. We looked into a few innovative effects and implications in the context of the findings for the two-dimensional nonautonomous framework of a PMSG because (a) the system variable dynamics are the same and disruption in the chaotic systems of the wind turbine system is identified, and (b) the similarity reveals that the short-memory has quite strange chaotic behaviour compared to the classical one. There are numerous unresolved issues that must be addressed. For example, despite the analysis presented here, a precise innovation can be explored using the work presented in [53, 54].

Use of AI tools declaration

The authors declare they have not used Artificial Intelligence (AI) tools in the creation of this article.

Acknowledgements

The authors acknowledge the Deanship of Scientific Research, Vice Presidency for Graduate Studies and Scientific Research, King Faisal University, Saudi Arabia, under project Grant No. 2213.

Conflict of interest

The authors declare no competing interests.

References

1. E. Muljadi, C. P. Butterfield, P. Migliore, Variable speed operation of generators with rotor-speed feedback in wind power applications, *J. Sol. Energy. Eng.*, **118** (1996), 270–277. https://doi.org/10.1115/1.2871793
2. S. A. de la Salle, D. Reardon, W. E. Leithead, M. J. Grimble, Review of wind turbine control, *Int. J. Control*, **52** (1990), 1295–1310. https://doi.org/10.1080/00207179008953597
3. L. Ren, F. Liu, Y. Jia, Active disturbance rejection control for chaotic permanent magnet synchronous generator for wind power system, *Proceedings of the 31st Chinese Control Conference*, China: Hefei, 2012, 6878–6882.
4. M. Messadi, A. Mellit, K. Kemih, M. Ghanes, Predictive control of a chaotic permanent magnet synchronous generator in a wind turbine system, *Chin. Phys. B*, **24** (2015), 010502. https://doi.org/10.1088/1674-1056/24/1/010502
5. C. H. Lin, Dynamic control for permanent magnet synchronous generator system using novel modified recurrent wavelet neural network, *Nonlinear Dyn.*, **77** (2014), 1261–1284. https://doi.org/10.1007/s11071-014-1376-3
6. F. Salas, F. Gordillo, J. Aracil, R. Reginatto, Codimension-two bifurcations in indirect field oriented control of induction motor drives, *Int. J. Bifurcat. Chaos*, **18** (2008), 779–792. https://doi.org/10.1142/S0218127408020641
7. C. Pezeshki, S. Elgar, R. C. Krishna, Bispectral analysis of possessing chaotic motion, *J. Sound Vib.*, **137** (1990), 357–368. https://doi.org/10.1016/0022-460X(90)90804-9
8. K. Miller, B. Ross, Fractional difference calculus, *Proceedings of the International Symposium on Univalent Functions, Fractional Calculus and Their Applications*, Nihon University, Koriyama, Japan, 1989, 139–152.
9. G. C. Wu, D. Baleanu, Discrete fractional logistic map and its chaos, *Nonlinear Dyn.*, **75** (2014), 283–287. https://doi.org/10.1007/s11071-013-1065-7
10. H. G. Sun, W. Chen, H. Wei, Y. Q. Chen, A comparative study of constant-order and variable-order fractional models in characterizing memory property of systems, *Eur. Phys. J. Spec. Top.*, **193** (2011), 185–192. https://doi.org/10.1140/epjst/e2011-01390-6

11. H. Zhang, F. Liu, M. S. Phanikumar, M. M. Meerschaert, A novel numerical method for the time variable fractional order mobile-immobile advection-dispersion model, *Comput. Math. Appl.*, **66** (2013), 693–701. https://doi.org/10.1016/j.camwa.2013.01.031

12. S. G. Samko, B. Ross, Integration and differentiation to a variable fractional order, *Integr. Transf. Spec. Funct.*, **1** (1993), 277–300. https://doi.org/10.1080/10652469308819027

13. C. F. Lorenzo, T. T. Hartley, Initialization, conceptualization, and application in the generalized fractional calculus, *Crit. Rev. Biomed. Eng.*, **35** (2007), 477–553. https://doi.org/10.1615/CritRevBiomedEng.v35.i6.10

14. G. C. Wu, Z. G. Deng, D. Baleanu, D. Q. Zeng, New variable-order fractional chaotic systems for fast image encryption, *Chaos*, **29** (2019), 083103. https://doi.org/10.1063/1.5096645

15. N. V. Kuznetsov, G. A. Leonov, T. N. Mokaev, A. Prasad, M. D. Shrimali, Finite-time Lyapunov dimension and hidden attractor of the Rabinovich system, *Nonlinear Dyn.*, **92** (2018), 267–285. https://doi.org/10.1007/s11071-018-4054-z

16. G. A. Leonov, N. V. Kuznetsov, Hidden attractors in dynamical systems. From hidden oscillations in Hilbert-Kolmogorov, Aizerman, and Kalman problems to hidden chaotic attractors in Chua circuits, *Int. J. Bifurcat. Chaos*, **23** (2013), 1330002. https://doi.org/10.1142/S0218127413300024

17. L. E. Ramirez, C. F. Coimbra, A variable order constitutive relation for viscoelasticity, *Ann. Phys.*, **519** (2007), 543–552. https://doi.org/10.1002/andp.200751907-803

18. H. Zhou, C. Wang, Z. Duan, M. Zhang, J. Liu, Timebased fractional derivative approach to creep constitutive model of salt rock, *Sci. Sin. Phys. Mech. Astron.*, **42** (2012), 310–318.

19. Y. F. Pu, W. X. Wang, J. L. Zhou, Y. Y. Wang, H. D. Jia, Fractional differential approach to detecting textural features of digital image and its fractional differential filter implementation, *Sci. China Ser. F: Inf. Sci.*, **51** (2008), 1319–1339. https://doi.org/10.1007/s11432-008-0098-x

20. M. Bohner, A. Peterson, *Dynamic equations on time scales: an introduction with applications*, Birkhäuser, Boston, 2001.

21. C. Goodrich, A. Peterson, *Discrete fractional calculus*, Springer, 2015.

22. L. Guo, X. L. Zhao, X. M. Gu, Y. L. Zhao, Y. B. Zheng, T. Z. Huang, Three-dimensional fractional total variation regularized tensor optimized model for image deblurring, *Appl. Math. Comput.*, **404** (2021), 126224. https://doi.org/10.1016/j.amc.2021.126224

23. L. Ren, J. Mou, S. Banerjee, Y. Zhang, A hyperchaotic map with a new discrete memristor model: design, dynamical analysis, implementation and application, *Chaos, Solitons Fract.*, **167** (2023), 113024. https://doi.org/10.1016/j.chaos.2022.113024

24. Y. Chen, J. Mou, H. Jahanshahi, Z. Wang, Y. Cao, A new mix chaotic circuit based on memristor–memcapacitor, *Eur. Phys. J. Plus*, **138** (2023), 78. https://doi.org/10.1140/epjp/s13360-023-03699-7

25. T. Ma, J. Mou, B. Li, S. Banerjee, H. Yan, Study on the complex dynamical behavior of the fractional-order Hopfield neural network system and its implementation, *Fractal Fract.*, **6** (2022), 637. https://doi.org/10.3390/fractalfract6110637

26. K. A Abro, A. Atangana, Mathematical analysis of memristor through fractal-fractional differential operators: a numerical study, *Math. Methods Appl. Sci.*, **43** (2020), 6378–6395. https://doi.org/10.1002/mma.6378
27. U. A. Aziz, A. Mukarram, K. A. Abro, Electroosmotic slip flow of Oldroyd-B fluid between two plates with non-singular kernel, *J. Comput. Appl. Math.*, **376** (2020), 112885. https://doi.org/10.1016/j.cam.2020.112885
28. Z. Li, J. B. Park, Y. H. Joo, B. Zhang, G. Chen, Bifurcations and chaos in a permanent-magnet synchronous motor, *IEEE Trans. Circ. Syst. I: Fundam. Theory Appl.*, **49** (2002), 383–387. https://doi.org/10.1109/81.989176
29. Z. Jing, C. Yu, G. Chen, Complex dynamics in a permanentmagnet synchronous motor model, *Chaos, Solitons Fract.*, **22** (2004), 831–848. https://doi.org/10.1016/j.chaos.2004.02.054
30. J. G. Lu, G. Chen, A note on the fractional-order Chen system, *Chaos, Solitons Fract.*, **27** (2006), 685–688. https://doi.org/10.1016/j.chaos.2005.04.037
31. S. Qureshi, A. Atangana, Mathematical analysis of dengue fever outbreak by novel fractional operators with field data, *Phys. A: Stat. Mech. Appl.*, **526** (2019), 121127. https://doi.org/10.1016/j.physa.2019.121127
32. G. C. Wu, M. Luo, L. L. Huang, S. Banerjee, Short memory fractional differential equations for new memristor and neural network design, *Nonlinear Dyn.*, **100** (2020), 3611–3623. https://doi.org/10.1007/s11071-020-05572-z
33. I. Podlubny, *Fractional differential equation*, San Diego: Academic Press, 1999.
34. A. A. Kilbas, H. M. Srivastava, J. J. Trujillo, *Theory an applications of fractional differential equations*, Amsterdam: Elsevier Science B.V., 2006.
35. N. R. O. Bastos, R. A. C. Ferreira, D. F. M. Torres, Discrete-time fractional variational problems, *Signal Process.*, **91** (2011), 513–524. https://doi.org/10.1016/j.sigpro.2010.05.001
36. D. Mozyrska, E. Girejko, Overview of fractional h-difference operators. In: A. Almeida, L. Castro, F. O. Speck, *Advances in harmonic analysis and operator theory*, Operator Theory: Advances and Applications, Vol. 229, Birkhäuser, Basel, 2013.
37. T. Abdeljawad, R. Mert, D. F. Torres, Variable order Mittag-Leffler fractional operators on isolated time scales and application to the calculus of variations, In: *Fractional derivatives with Mittag-Leffler kernel*, Springer: Cham, Switzerland, 2019, 35–47.
38. W. Deng, Short memory principle and a predictor–corrector approach for fractional differential equations, *J. Comput. Appl. Math.*, **206** (2007), 174–188. https://doi.org/10.1016/j.cam.2006.06.008
39. M. Al. Qurashi, S. Rashid, F. Jarad, E. Ali, R. H. Egami, Dynamic prediction modelling and equilibrium stability of a fractional discrete biophysical neuron model, *Results Phys.*, **48** (2023), 106405. https://doi.org/10.1016/j.rinp.2023.106405
40. Z. Wang, H. Xia, Y. X. Li, X. N. Song, A new image encryption algorithm based on the fractional-order hyperchaotic Lorenz system, *Chinese Phys. B*, **6** (2013), 010504. https://doi.org/10.1088/1674-1056/22/1/010504

41. F. Liu, P. Zhuang, V. Anh, I. Turner, K. Burrage, Stability and convergence of the difference methods for the space-time fractional advection-diffusion equation, *Appl. Math. Comput.*, **191** (2007), 12–20. https://doi.org/10.1016/j.amc.2006.08.162

42. X. J. Yang, *Advanced local fractional calculus and its applications*, Singapore: World Science Publisher, 2012.

43. H. G. Sun, W. Chen, Y. Q. Chen, Variable-order fractional differential operators in anomalous diffusion modeling, *Phys. A*, **388** (2009), 4586–4592. https://doi.org/10.1016/j.physa.2009.07.024

44. M. D. Ortigueira, D. Valrio, J. T. Machado, Variable order fractional systems, *Commun. Nonlinear Sci. Numer. Simul.*, **71** (2019), 231–243. https://doi.org/10.1016/j.cnsns.2018.12.003

45. M. Feckan, Y. Zhou, J. R. Wang, On the concept and existence of solution for impulsive fractional differential equations, *Commun. Nonlinear Sci. Numer. Simul.*, **17** (2012), 3050–3060. https://doi.org/10.1016/j.cnsns.2011.11.017

46. I. Petras, Fractional-order memristor-based Chua's circuit, *IEEE Trans. Circ. Syst. II, Express Briefs*, **57** (2010), 975–979. https://doi.org/10.1109/TCSII.2010.2083150

47. W. Deng, Smoothness and stability of the solutions for nonlinear fractional differential equations, *Nonlinear Anal.*, **72** (2010), 1768–1777. https://doi.org/10.1016/j.na.2009.09.018

48. M. S. Tavazoei, M. Haeri, Unreliability of frequency-domain approximation in recognising chaos in fractional-order systems, *IET Signal Process.*, **1** (2007), 171–181.

49. I. Petras, A note on the fractional-order Volta's system, *Commun. Nonlinear Sci. Numer. Simul.*, **15** (2010), 384–393. https://doi.org/10.1016/j.cnsns.2009.04.009

50. G. C. Wu, D. Baleanu, Jacobian matrix algorithm for Lyapunov exponents of the discrete fractional maps, *Commun. Nonlinear Numer. Simul.*, **22** (2015), 95–100. https://doi.org/10.1016/j.cnsns.2014.06.042

51. Y. Y. Hou, Controlling chaos in permanent magnet synchronous motor control system via fuzzy guaranteed cost controller, *Abstr. Appl. Anal.*, **2012** (2012), 650863. https://doi.org/10.1155/2012/650863

52. K. Rajagopal, A. Karthikeyan, P. Duraisamy, Chaos suppression in fractional order permanent magnet synchronous generator in wind turbine systems, *Nonlinear Eng.*, **6** (2016), 79–87. https://doi.org/10.1515/nleng-2016-0059

53. X. M. Gu, H. W. Sun, Y. L. Zhao, X. Zheng, An implicit difference scheme for time-fractional diffusion equations with a time-invariant type variable order, *Appl. Math. Lett.*, **120** (2021), 107270. https://doi.org/10.1016/j.aml.2021.107270

54. R. Garrappa, A. Giusti, F. Mainardi, Variable-order fractional calculus: a change of perspective, *Commun. Nonlinear Sci. Numer. Simul.*, **102** (2021), 105904. https://doi.org/10.1016/j.cnsns.2021.105904